Project 056 Turbine Cooling Through Additive Manufacturing

The Pennsylvania State University

Project Lead Investigator

Reid A. Berdanier
Associate Professor
Department of Mechanical Engineering
The Pennsylvania State University
NARCO Building, CATO Park, Room 148
3127 Research Drive
State College, PA 16801
(814) 863-3972
rberdanier@psu.edu

University Participants

The Pennsylvania State University (Penn State)

- P.I.s: Prof. Reid A. Berdanier, Prof. Stephen Lynch, Prof. Karen Thole
- FAA Award Number: 13-C-AJFE-PSU-126
- Period of Performance: February 5, 2020, to September 30, 2026
- Tasks:
  1. Manufacture and test existing FAA Continuous Lower Energy, Emissions, and Noise (CLEEN) II blade designs.
  2. Design new double-wall cooling technologies.
  3. Manufacture and test new double-wall cooling designs for linear cascade.
  4. Manufacture and Test AM NExT Blades with Varying Roughness
  5. Develop Correlations for Realistic Turbine Roughness

Project Funding Level

The Federal Aviation Administration (FAA) has provided $1,800,000 of funding to date. In-kind cost-sharing of $1,800,000 has been provided by Pratt & Whitney ($1,500,000), and Penn State ($300,000).

Investigation Team

Prof. Reid A. Berdanier, All Tasks
Prof. Karen A. Thole (co-P.I.), All Tasks
Prof. Stephen Lynch (co-P.I.), Tasks 2, 3, and 5
Assoc. Res. Prof. Michael Barringer, (staff scientist), Task 1 and 4
Asst. Res. Prof. Matthew Meier, (staff scientist), Task 1 and 4
Scott Fishbone, (project manager, departed), Task 1
Justin Brumberg (staff scientist), Task 1 and 4
Tom Houck (project manager), Task 1 and 4
Jeremiah Bunch, (laboratory technician), Task 1 and 4
Liam Boyd, (graduate student, graduated), Tasks 2 and 3
Nicholas Gailey, (graduate student, graduated), Task 1
Ethan Bonn, (graduate student), Task 1
Abigail Altland, (graduate student), Task 5
Matthew Stuber, (graduate student), Task 5
Benjamin Bizzak, (graduate student), Task 4

Project Overview

Gains in the cooling performance of cooled turbine airfoils directly affect the efficiency and durability (lifetime) of turbine engines and therefore are the subject of substantial development. Currently, many cooling designs for turbine airfoils use complex micro-channels placed within the wall of the airfoil to extract heat—a design known as double-wall cooling. However, the geometric complexities (and thus the effectiveness) of the micro-channels are limited by the current design space available through the use of conventional investment casting and core tooling methods to manufacture relatively small intricate internal cooling features. This project will investigate potential thermal performance and aerodynamic efficiency improvements made possible by exploring the expanded cooling design space opportunities by directly fabricating complex cooling geometries with three-dimensional laser powder bed fusion (L-PBF), a commonly used metal-based additive manufacturing (AM) method. L-PBF AM has begun to find many uses in the gas turbine industry, particularly because of the new design space enabled by this new fabrication method. However, the ability to manufacture high-efficiency, intricate, complex double-wall cooling airfoils design concepts is unknown. This research would generate some of the first thermal performance data at engine-relevant conditions comparing traditional cast airfoils to advanced airfoils manufactured through L-PBF AM. Understanding the potential of new innovative geometric heat transfer cooling design features coupled with unique airfoil cooling configurations will serve as an important guide for future investments in advanced manufacturing and cooling design technologies.

Task 1 – Manufacture and Test Existing FAA CLEEN II Blade Designs

The Pennsylvania State University

Objective

The objectives of this task are to measure the as-manufactured shape of FAA CLEEN II turbine blade airfoils with X-ray computed tomography (CT), and to use that information to fabricate additively manufactured copies for direct comparison at the rotating turbine facility at Penn State. The outcomes of this effort will be to (a) provide a direct back-to-back comparison of cast versus additively manufactured airfoils, (b) identify the unknown challenges in creating double-wall designs via AM and translating them into cast parts for commercialization, and (c) learn about and document the design, fabrication, and testing of additive blades that will spin at engine-relevant conditions.

Research Approach

AM Blade Inspections and Testing Preparation

Testing of the FAA CLEEN II blade designs has been completed within the Steady Thermal Aero Research Turbine (START) rig. A low, mid, and high blade coolant flow rate was achieved over the test campaign. CT scans and blue light scans of an ideal geometric FAA CLEEN II cast blade were used to generate a solid model for the manufacturing of the AM blade set. Infrared (IR) images were taken of every blade while rotating at 10,000+ rpm and initial observations were summarized in previous reports. The detailed analysis to understand the specific impact of AM versus cast blade performance is continuing, and those results are summarized in the current report.

Additional post-test coolant flow studies were conducted to better understand how much coolant was being supplied to specific sections of the blade. Figure 1 illustrates the flow parameter apparatus and measured data normalized by the maximum flow parameter across a representative range of pressure ratios for the trailing edge slots only. This was conducted by blocking all cooling holes and the tip region, while also blocking the inlet to all coolant feed channels except the one feeding the trailing edge slots, as shown in Figure 1a. The blades were then pressed into a custom-made gasket that sealed the root of the blade while a flowmeter measured the supplied pressure, temperature, and mass flow rate below the root. Figure 1b shows the cast blades have a greater flow parameter compared to the AM blades, where a greater flow parameter corresponds to more mass flow being supplied through the blades. This observation initially supports fundamental expectations that AM roughness will add to the pressure drop behavior and limit flow capacity.

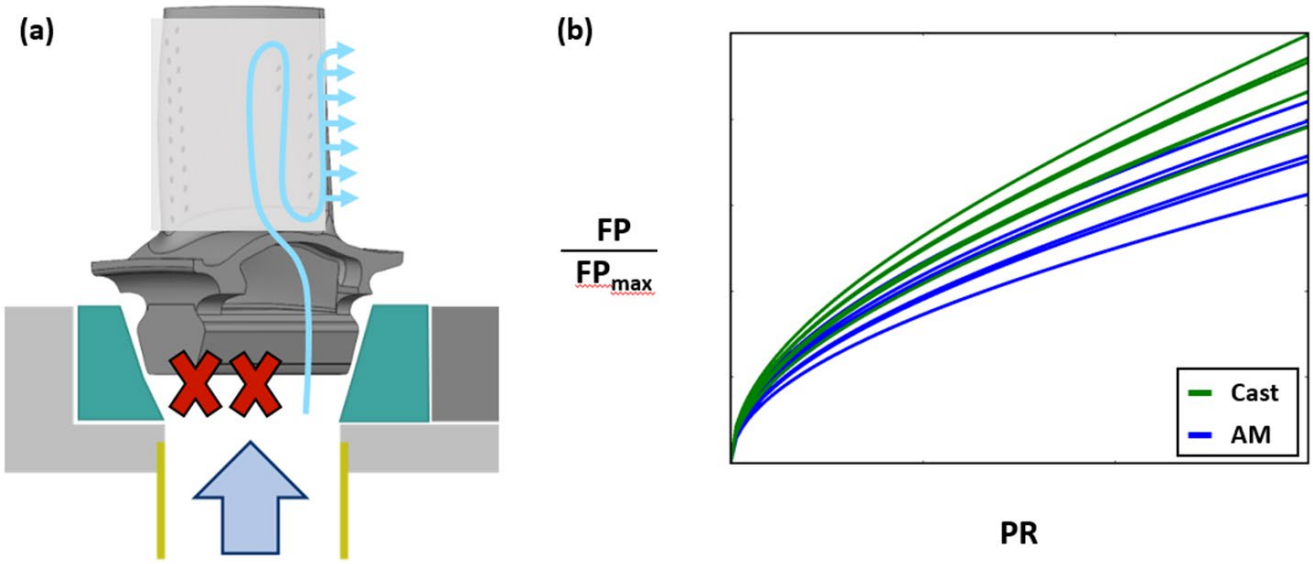

Figure 1. (a) Custom flow parameter apparatus representing trailing edge slot flow measurements (b) Post operation flow parameter measurements of the trailing edge slots for a subset of the turbine blade wheel. AM: additive manufacturing, FP: flow parameter, PR: pressure ratio.

It is important to understand how specific cooling flow rates compare to the measured overall cooling effectiveness (ϕ). The region to be analyzed on the pressure side was chosen to be upstream of the cooling hole row and over the internal trailing edge serpentine passage only, as shown in Figure 2a. Data comparing $\overline{\overline{\phi}}$ to flow parameter are shown in Figure 2b as three distinct groups for each blade manufacturing type corresponding to the three flow conditions measured within START. Differences within a blade group are expected due to manufacturing defects as shown by the separation between the datapoints. Any shift along a calculated polynomial curve fit is assumed to be due to the change in flow rate, while vertical shifts in thermal performance are due to internal geometric differences. When further analyzing these results, CT scans will be used to better determine which geometric changes impacted the blade surface temperatures.

Due to the AM blades having the same design as a singular cast blade, it is expected that the AM blades should have similar cooling performance for similar mass flow rate to that particular blade. However, it is important to understand how the whole group of manufactured blades performs as well. The polynomial curve fit for each blade was used to predict the thermal performance at a set flow parameter to provide similar flow rate comparisons between the two manufacturing types, as shown in Figure 2c. These data show larger variations in thermal performance for the AM blades, which could be caused by the manufacturing process. Again, CT scans and additional flow measurements will provide information on internal defects, i.e., internal cooling channel breakthroughs, internal rib geometries, and blade thickness, all of which have an impact on the surface temperature of the blade. This investigation is ongoing and is expected to advance further during the next reporting period.

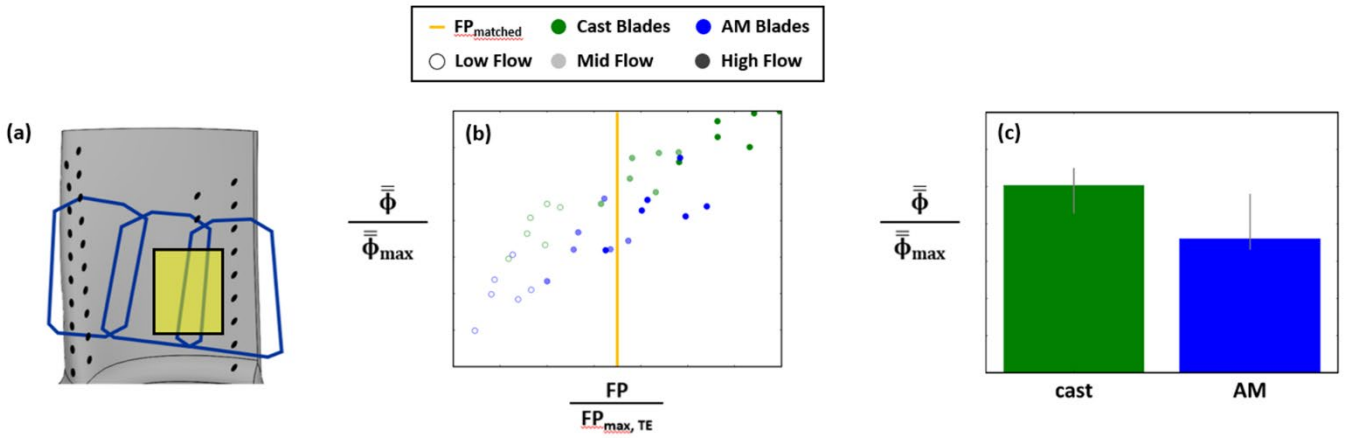

Figure 2. (a) Area-averaged region of interest on the pressure side of the blade, selected to compare (b) the measured post operation flow rate through the blade to the surface temperature and (c) the predicted normalized overall effectiveness at a target FP. AM: additive manufacturing, FP: flow parameter.

CT scans were analyzed to gather information about the blade's material thickness. Seven distinct locations along the blade's surface were measured between three cast blades and three AM blades. Shown in Figure 3 is measured wall thickness normalized by wall thickness design intent at a single span height along the blade's surface. It is important to note that the design intent wall thickness for cast blades was the FAA CLEEN II design, while the design intent wall thickness for AM blades was the solid model generated from the CT scans and blue light scans of the ideal geometric FAA CLEEN II blade as previously described. AM blades show less variability in wall thickness across the entire surface of the blades analyzed, which is expected due to the manufacturing process. Knowing the wall thicknesses between cast and AM blades is vital in understanding the exact thermal resistance felt by the blade material, which will help determine the specific impact thickness has on the measured cooling performances.

Initial thermal differences were discussed in the quarter (Q)1 fiscal year (FY)25 report by linking mass flow rate to area averaged effectiveness, which showed that the AM blades underflowed the cast blades, in addition to underperforming thermally. However, it was found that all the blades had internal kiss-ins which allowed coolant to leak between internal passages. This means that the partial flow parameters measured are not the same between bench flow tests and START rig tests. Therefore, a new thermal assessment has been conducted, which takes set span ϕ surface wraps along the entire blade, as shown in Figure 4 (high flow test condition only). The range of AM and cast blades, regions of blue and green, are bounded by their respective max and min values measured at the span indicated by the yellow line across the blade cartoon. The orange line represents the thermal performance of the cast blade that was used to generate the solid model for the manufacturing of the AM blade set. It can be noticed that the AM blades pressure side trailing edge generally has lower thermal performance when compared to cast blade set. But, when shifting from the trailing edge to the leading edge, the AM blades are observed to have greater thermal performance relative to the cast blades. This shift is directly due to the internal kiss-ins and slight design differences between the cast and AM blades, which caused the AM blade leading-edge region to have greater mass flow rate, thus driving temperatures lower.

Determining the wall thickness measurements impact on the IR thermal measurements requires a one-dimensional nodal network of resistances. Equation 1 relates the IR measured temperatures (left hand side) to the rearranged nodal network (right hand side).

$$\frac{T_{mgp}-T_s}{T_{mgp}-T_c} = \phi = \frac{\frac{1}{h_e}}{\frac{1}{h_e}+\frac{t_{wall}}{k_{material}}+\frac{1}{h_i}} = \frac{R_1}{R_1+R_2+R_3} \quad \text{(Eq. 1)}$$

T_{mgp} and T_c are circumferential temperature measurements taken from the main gas path and blade cooling flow path respectively, while T_s is the measured blade surface temperature. The external and internal convection coefficients are

represented by h_e and h_i and the specific blade material thermal conductivity is $k_{material}$. It is desired to understand which resistance- R_1, R_2, or R_3- is the primary driver of the measured thermal difference. With known wall thickness at discrete locations along the blade, and thermal measurements at those same locations, IR measurements can be related to R_2. Figure 5 shows the averaged cooling performance at the discrete locations used for thickness measurements plotted against the averaged wall thickness at the same location. Tracking regions that had similar wall thickness differences between the AM and cast blades- -28% (triangle), -10% (square), and 85% (right facing triangle)-there is no noticeable trend between these shapes. This indicates that the wall thickness does have an impact on measured surface temperatures but is not the primary driver of thermal differences measured between cast and AM blades.

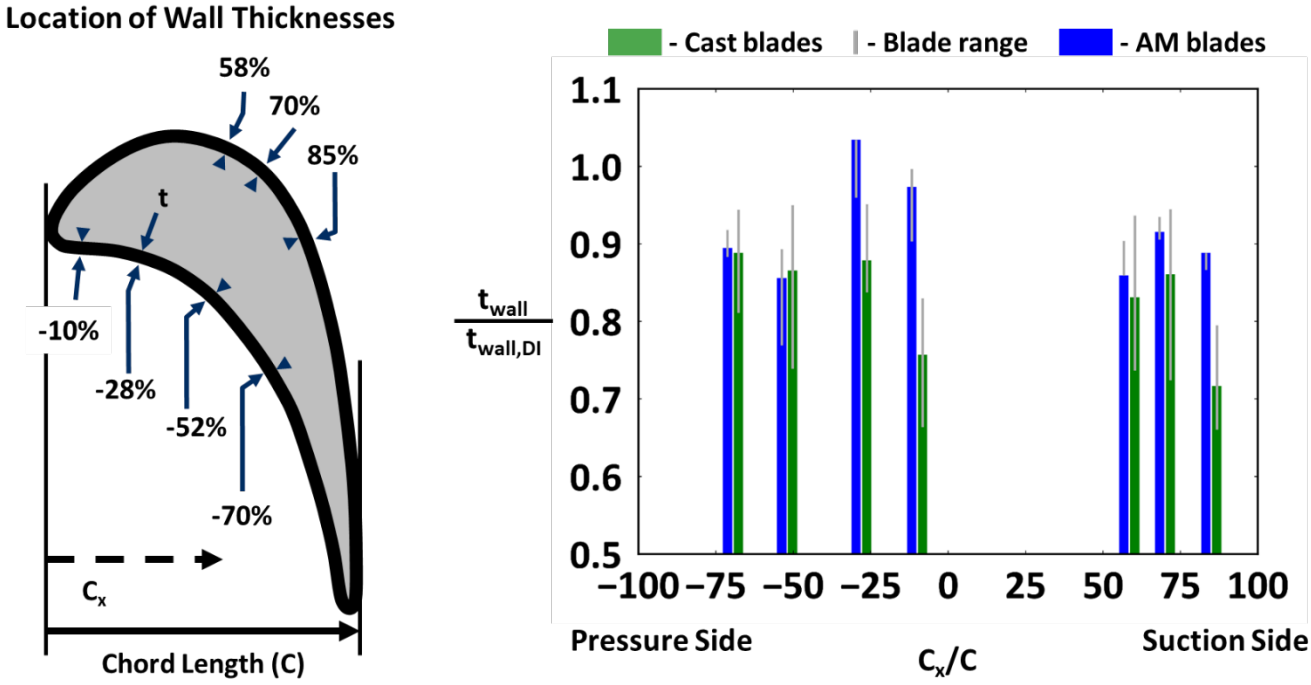

Figure 3. Blade wall thickness at seven distinct locations along the pressure side and suction side of the blade.

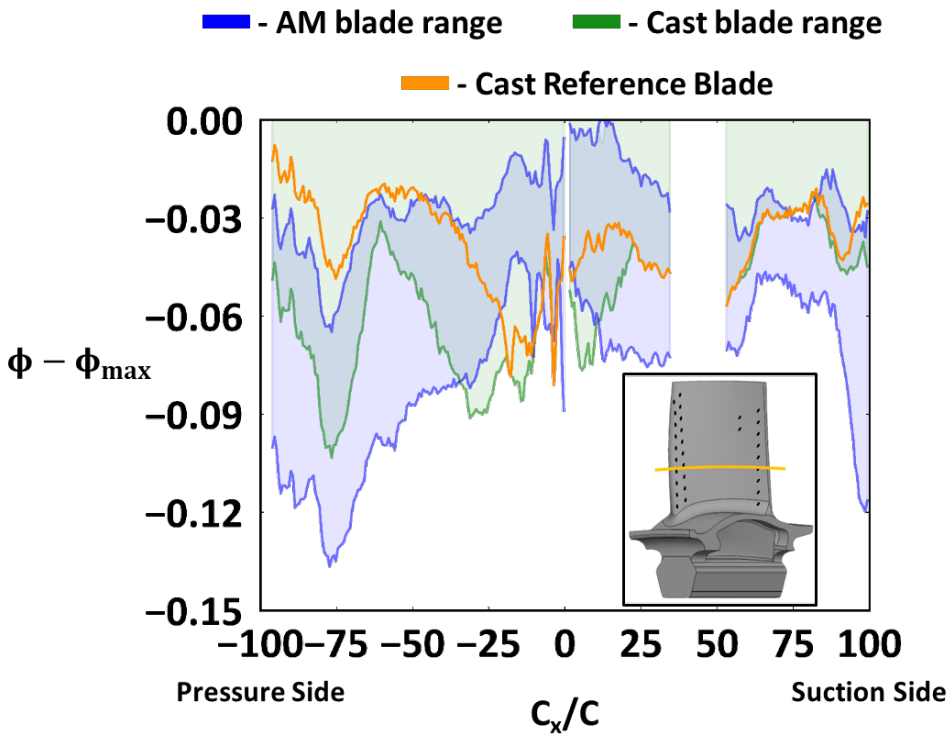

Figure 4. Blade cooling performance at the high flow test condition for a set span height across the entire surface of the airfoil. AM: additive manufacturing, C: chord length.

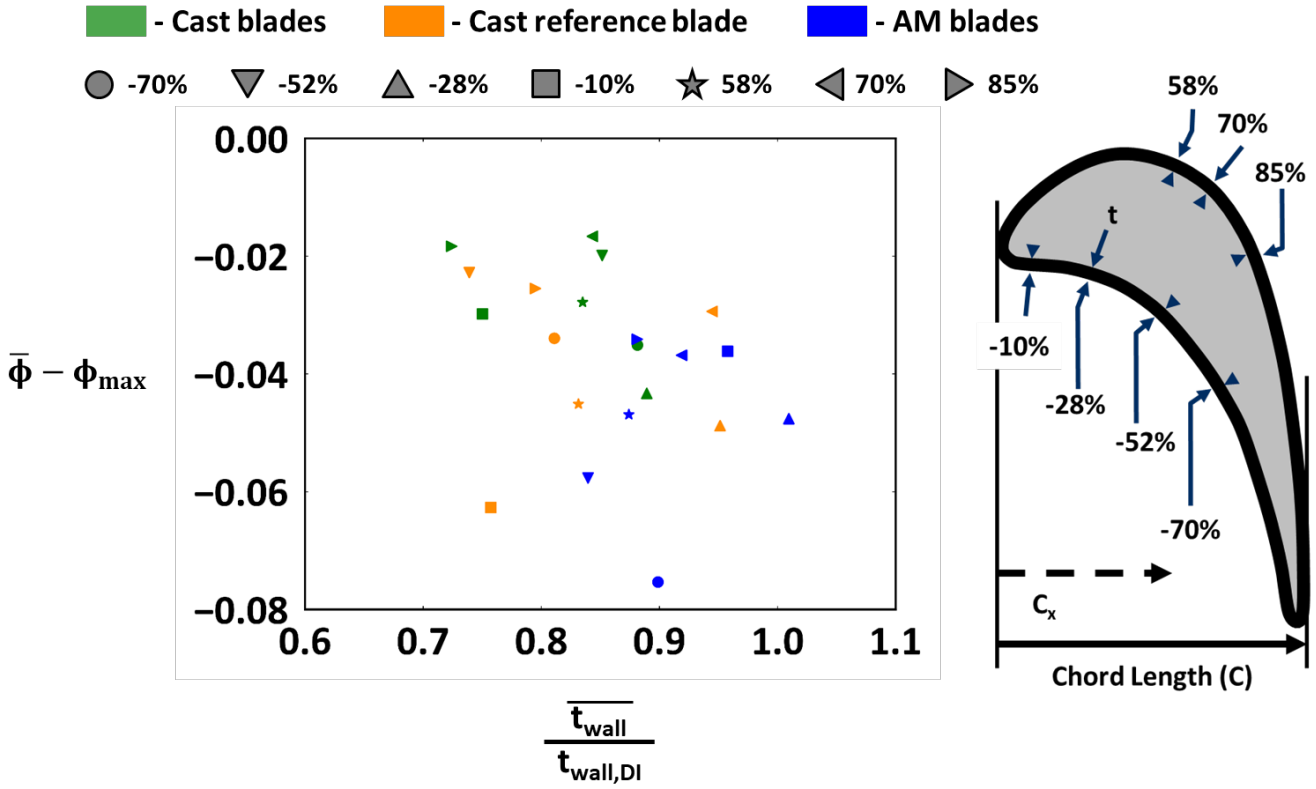

Figure 5. Averaged thermal performance compared to average wall thickness at seven discrete locations for a set span height. AM: additive manufacturing.

Future analysis is planned to understand how the other resistances, R_1 and R_3, impact cooling performance. It is known that AM produces rougher internal surfaces, which could enhance heat transfer and impact pressure loss through cooling channels. It is expected that the internal cooling coefficient will have the largest impact on blade surface temperatures based on preliminary calculations using simplified geometries. To help verify this prediction, Nusselt number surface roughness augmentations will be applied to calculated cooling performances, which will be directly compared to the measured cooling performances.

Following initial data analysis reported in prior quarterly reports, continued analysis was performed in Q3 FY25 to evaluate the cast versus AM comparison of CLEEN II blade designs. Figure 6a and 6b show an illustration of the external cooling features of the blades, along with the print direction used for this study for the AM blade set. Both the cast and AM blade sets comprised rib turbulated leading-edge cavity and serpentine cooling channels, internal impingement slots between the serpentine channels, and a trailing edge pin-fin array. Also shown in Figure 6c is an illustrated internal cooling passage that includes V-shaped rib turbulators. It is important to note that the internal cooling passage only has turbulators within the airfoil portion of the blade, location 3 in Figure 6c; there were no turbulators in the root portion of the blade that supplies the blade coolant, location 1 in Figure 6c. The region located between non-turbulated inlet portion of the blade and the turbulated airfoil portion of the blade is referred to throughout this section as location 2, shown in Figure 6c.

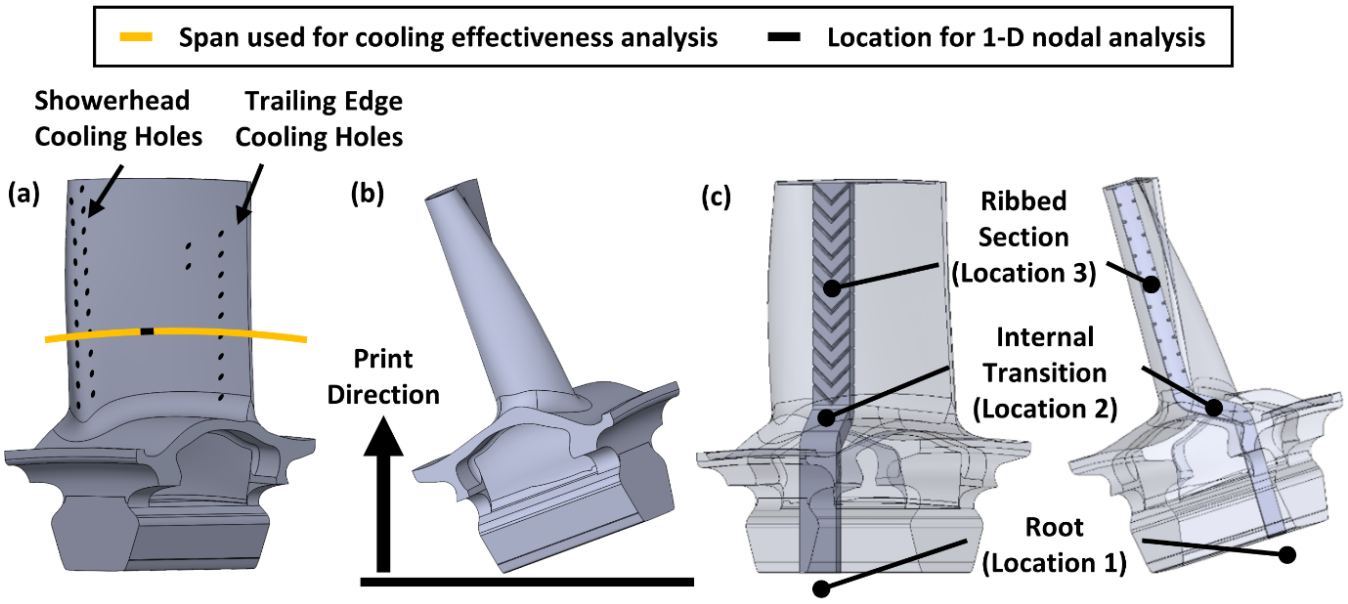

Figure 6. Graphical representations of an engine scale turbine blade with a generic internal cooling channel and external cooling hole locations. Also shown is the print direction used for the AM blade set and the specific span used for cooling effectiveness surface wraps, one-dimensional (1D) nodal network analyses, and predictive surface temperature analysis. Turbine blade geometries are for illustrative purposes only.

Using the spatially-resolved IR measurements, data were extracted for a fixed span location depicted in Figure 6a to compare cast and AM blades. Figure 7 shows the temperature distributions for both blade set ranges, with the AM blade set in blue and the cast blade set in green in terms of a non-dimensional $\Delta\phi$ value. Different from the analysis shown in Q2 FY25 report, Figure 7 evaluates the difference between the AM blade relative to the cast reference blade. Comparisons were made by normalizing the non-dimensional temperature data by that of the cast reference blade such that the orange line shows the datum. For this study, ϕ was defined using the cooling temperature located at location 1 and is shown by Equation 2. The main gas path temperature, T_∞, and coolant temperature, $T_{c,1}$, used in this chapter was in the relative reference frame. It was also important to distinguish T_c within this section was different from the coolant temperature discussed later in this section and therefore was marked with a location 1 indicator. All ϕ values, however, presented in this section are calculated using the root coolant temperature from location 1 and are also marked accordingly with a location 1 indicator, with the cast reference blade referred to as $\phi_{1,\mathrm{ref}}$ throughout this chapter.

$$\phi_1 = \frac{T_\infty - T_s}{T_\infty - T_{c,1}} \quad \text{(Eq. 2)}$$

The general shape of cooling performance between the cast and AM blades was similar along the whole surface except around C_x/C = -65% shown in Figure 4. In this region, the cast blades converged toward the cast reference blade, and then immediately diverged towards the trailing edge, C_x/C = -100%. This was a result of the internal impingement slots located between the serpentine passages. CT scans of this region of both blade sets revealed that the AM impingement slots had large downskin dross formations partially blocking the impingement passage. With the internal walls conducting heat from one side of the blade to the other, reduced cooling means less ability to convect heat out of the internal wall. However, there only appears to be a local impact due to the impingement slots, with the overall range of performance for the cast blade set matching the overall range of the AM blade set just downstream at C_x/C = -75%.

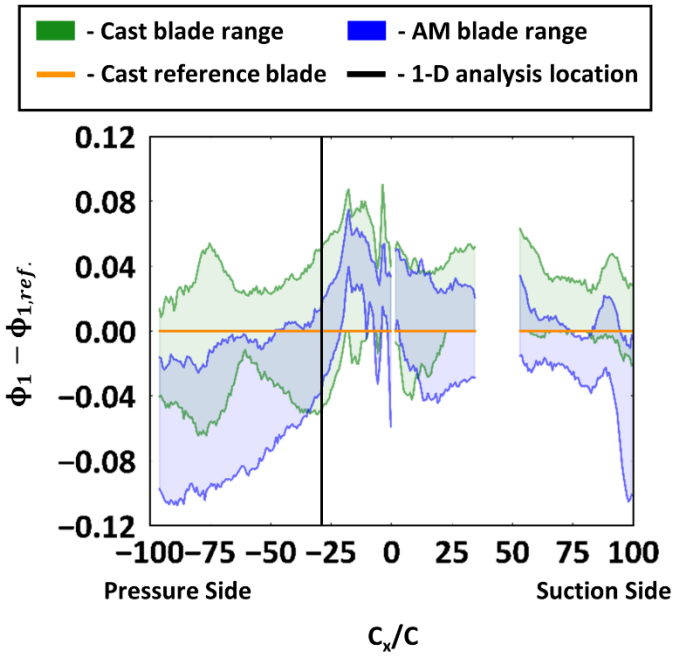

Figure 7. Blade cooling effectiveness ranges normalized by the AM design intent blade's cooling performance. AM: additive manufacturing, C: chord length.

The coolant temperature, $T_{c,3}$, was calculated using a discretized energy balance method for each manufacturing method, respectively. For this calculation, internal wall temperatures were required at three discrete locations – the root of the blade at location 1, where the internal passage transitions from smooth to a rib turbulated wall as shown in Figure 6c at location 2, and at 30% span as shown in Figure 6a at location 3. The surface temperatures at the blade root were calculated from isentropic flow relations converting cooling flow supply conditions to the relative frame of reference as the flow was swirled and onboarded to the blade disk. For this analysis, it was assumed that the coolant temperature at the blade root was equal to the surface temperatures at the blade root. IR images and external wall heat flux predictions were used to calculate the internal wall temperature at both the transition region and 30% span, locations 2 and 3, respectively. Using a discretized energy balance method for the two regions of the blade, smooth and rib-turbulated, and a linear internal wall temperature heat up, the coolant for the AM blades was calculated to be hotter at location 3 compared to the cast blades. This was expected due to the AM roughness throughout the full channel, including the region without ribs, within the blade. Equation 3 provides a non-dimensional comparison of the coolant heat up internally. The calculated difference of internal heat up was $\theta_{AM} - \theta_{cast}$ = -0.049. This result meant that the AM blade set had 5% less coolant potential than the cast blade set at location 3 with respect to the internal cooling temperatures.

$$\theta = \frac{T_\infty - T_{c,3}}{T_\infty - T_{c,1}} \quad \text{(Eq. 3)}$$

Recall that ϕ_1 is calculated using the location 1 coolant temperature, $T_{c,1}$, but the one-dimensional (1D) network utilizes the coolant temperature at location 3, $T_{c,3}$. The increase of calculated surface temperature for the AM blade set only when using the calculated cast coolant temperature, $T_{c,3,cast}$, compared to using the hotter calculated AM coolant temperature, $T_{c,3,AM}$, was a 4.5% decrease in ϕ_1. When the appropriate calculated coolant temperatures and literature driven correlations were used, the cast blades had a deviation of $\phi_{1,calculated} - \phi_{1,measured}$ = -0.002 on average, while the AM blades showed $\phi_{1,calculated} - \phi_{1,measured}$ = 0.006 on average. Both calculated surface temperatures were within measurement uncertainties. This analysis shows the importance of accounting for the additional roughness of the AM channel in closing the loop of understanding the thermal performance of AM and cast blades.

The 1D analysis provided a method for understanding the applicability of previously reported literature correlations derived in lower TRL facilities for use in a gas turbine blade analysis. While this analysis showed similar calculated ϕ_1 values to that of the measured ϕ_1 values, it was highly dependent on existing literature correlations and predicted data for location 2 on the blades surface. The limitations of this analysis were highlighted when the 1D network was applied to a region of the blade where no existing temperatures or correlations were available. This finding suggested that the entire blades surface temperature is needed to properly account for location 2 internal wall temperature, either measured or predicted. Also, ensuring internal convection correlations are acquired for geometries that match the end desired turbine blade product is essential for proper internal heat up analysis, which in turn means proper cooling effectiveness calculations.

Task 2 – Design New Double-wall Cooling Technologies

The Pennsylvania State University

Objective

The objective of this task is to develop novel double-wall cooling designs that feature the microchannel concepts being explored in the literature and which can be achieved via AM. The designs will be generated with advice from Pratt & Whitney, so that the concepts can be leveraged for commercialization. The designs will be packaged into cascade test articles that will be measured in the high-speed linear cascade at Penn State with IR thermography.

Research Approach

Design of Linear Cascade Test Articles

This task was completed in 2022 with final delivery of all high-speed cascade test articles to Penn State.

Task 3 – Manufacture and Test Novel Double-wall Cooling Designs for Linear Cascade

The Pennsylvania State University

Objective

The objective of this task is to measure the performance of the AM microchannels in the linear cascade airfoil and rank the performance of the novel geometries. This process includes measuring the pressure drop and the surface temperature of the airfoils with the novel microchannel geometries. Subsequent evaluation is conducted through computational fluid dynamics (CFD) investigations of the performance to understand physics and predictive capabilities of modern design tools.

Research Approach

Experimental Testing of Linear Cascade Hardware

This subtask was completed in 2024 and reported in a previous annual report. Blades were tested at a range of exit Mach and Reynolds numbers, with different amounts of internal cooling flow, and surface temperatures were measured using a calibrated infrared camera.

Computational Simulation of Linear Cascade Hardware

This task involved computational simulations of experimentally tested microchannel cooling designs from prior cascade tests. The goal of this task was to determine the accuracy of design-level conjugate CFD to predict the performance of the novel microchannel designs. To do this, a computational model of the single test blade was generated. Figure 8 shows the computational domain, with periodic sidewalls to simulate the periodic conditions of the high-speed linear cascade. The inlet of the domain was prescribed with stagnation pressure and temperature conditions from the experiments, and the outlet of the domain was prescribed with a static pressure also from the experiments to achieve the desired exit Mach number. The airfoil (cartoon shown due to proprietary nature of the actual airfoil design) had cooling channels based on the design intent of the various microchannel designs. The coolant inlet mass flow and temperature conditions were specified at the base of the airfoil to match test conditions. To conduct a conjugate analysis (prediction of metal temperature in the CFD), the domain included both the fluid volume inside the microchannels and around the blade but

also the solid domain of the blade material, connected by an interface that matches temperature and heat flux. All other walls (top endwall, bottom endwall) were specified as adiabatic and no-slip.

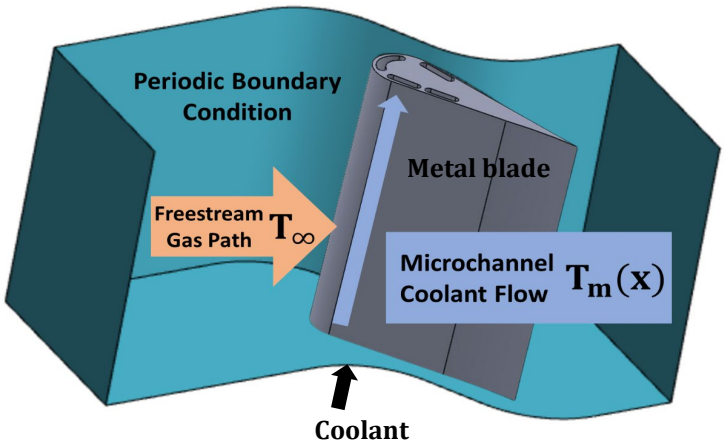

Figure 8. Computational domain for conjugate computational fluid dynamics analysis of microchannel cooled blade.

The solution approach was a steady Reynolds Averaged Navier Stokes (RANS) simulation in STAR CCM+,®[1] an industry standard design code. The fluid domain was modeled as an ideal gas with Sutherland's law for viscosity and thermal conductivity, and the solid domain was modeled as Inconel with constant thermal conductivity based on typical values for Inconel® 718 (the material the blades were constructed from). A coupled solver (simultaneous solution of all conservation equations) with second-order accuracy was chosen. To ensure iterative convergence, residuals of conservation equations were tracked, as well as mass-averaged outlet total pressure and surface average blade outer surface temperature. In general, the solution was iterated for more than 4,000 iterations until the residuals stopped changing and the other monitors were constant to within 1%. Work in prior years of this project indicated the necessary mesh size to achieve grid convergence, with approximately 3.7M cells for the empty microchannel simulations, and 10.4M cells for microchannels with internal geometries.

Figure 9 shows a comparison of computationally predicted results for nondimensional surface temperature of the blade metal (also known as overall cooling effectiveness), compared to the same experimental cases, for high and low microchannel flow rates. The cartoon on the left indicates how the results are "unwrapped" around the surface of the blade so that both sides of the blade can be presented in the figure. The external conditions for these cases were fixed at an exit Mach of 0.81 and an exit Reynolds number of 340,000.

In comparing Figures 9a to 9b, the level of nondimensional cooling of the metal decreases as the coolant flow rate decreases from a Reynolds number of 20,000 to a Reynolds number of 6,000. This is expected, since the hot gas conditions are unchanging, but the internal cooling convection decreases with Reynolds number. When comparing the computational predictions to the experiment at a given Reynolds number, there is generally good agreement in the trends of cool regions located around microchannels (dark blue) and warm regions (orange colors) that are downstream of the microchannel cooled region. The good agreement in external metal surface temperature was somewhat unexpected since the CFD does not model the as-manufactured surface roughness of the empty microchannels, but the results here indicate that the surface roughness is not a significant contribution to internal convective heat transfer for these microchannels.

® SimCenter and STAR CCM+ are registered trademarks of Siemens Industry Software NV, Leuven, Belgium.
[1] SimCenter STAR CCM+ is a comprehensive engineering simulation software that uses CFD and multiphysics technology to help engineers design and optimize products across a wide range of industries.
® Inconel is a registered trademark of Huntington Alloys Corporation, Huntington, West Virginia.

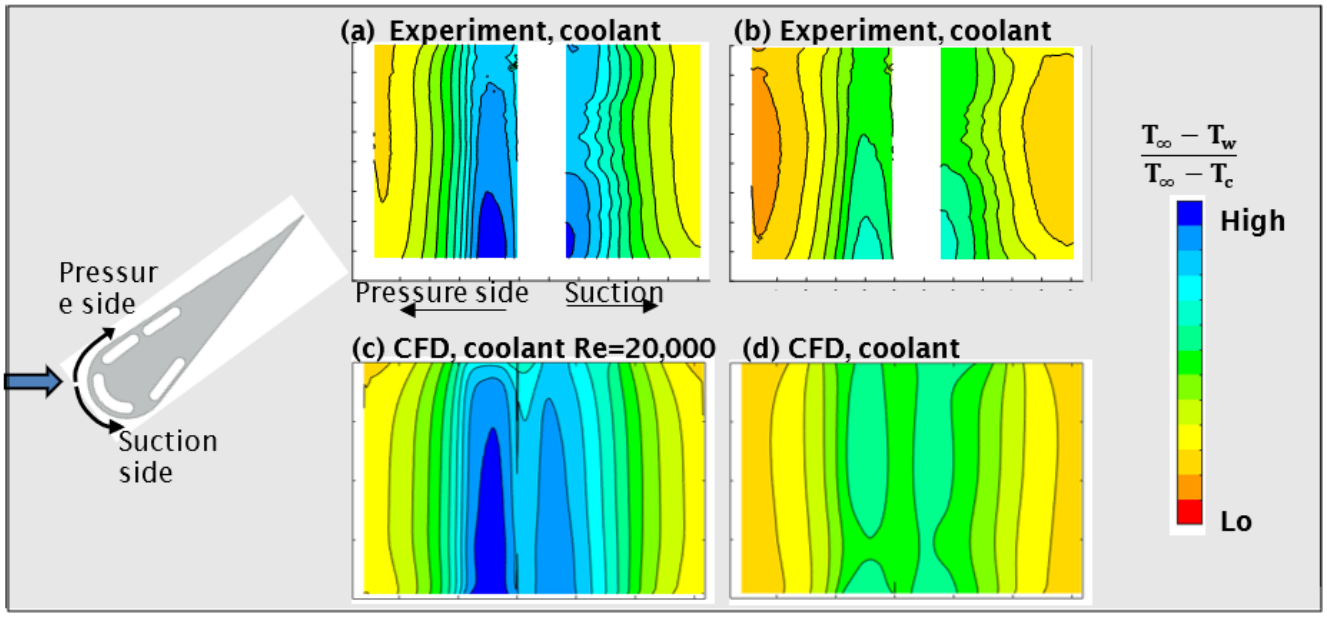

Figure 9. Comparison of experimentally measured nondimensional metal temperature (a,b) versus computationally predicted metal temperature (c,d) for high (Re=20,000) and low (Re=6,000) microchannel flow rates, for empty microchannels. CFD: computational fluid dynamics; Re: Reynolds number.

Other microchannels were also modeled in the conjugate CFD, including the w-rib design. Figure 10 shows a comparison of the experiment at a given coolant channel Reynolds number to the CFD at the same condition. Here, the CFD significantly overpredicts the cooling performance of the W-rib design, with a much cooler region (high overall cooling effectiveness) around the leading edge of the blade.

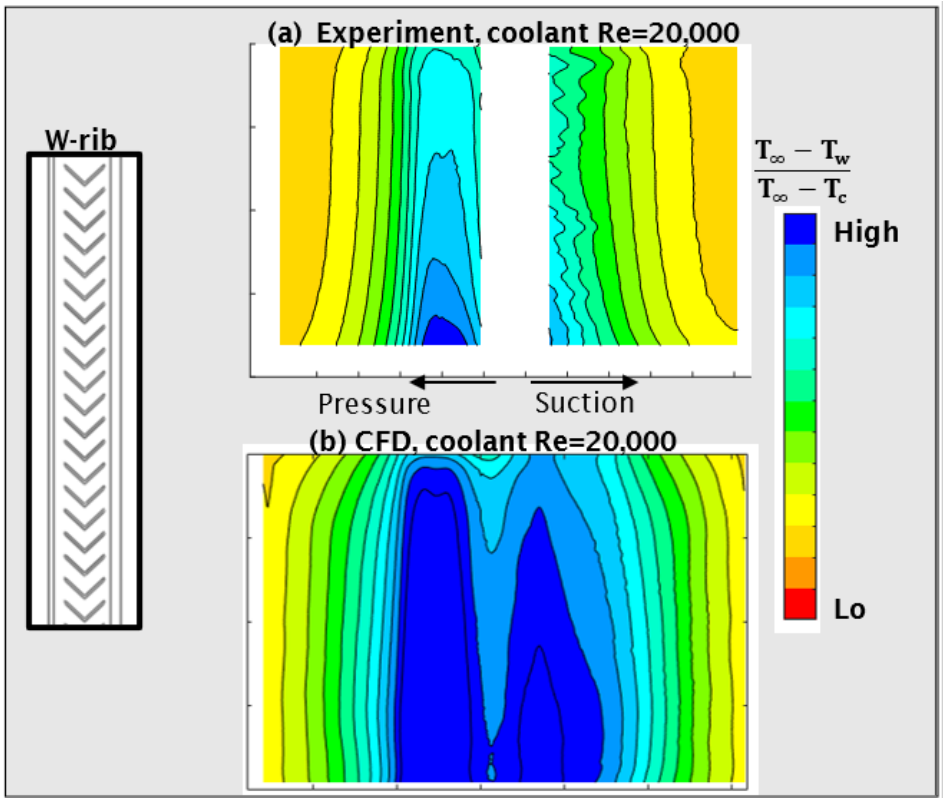

Figure 10. Comparison of experimentally measured nondimensional metal temperature (a) versus computationally predicted metal temperature (b) for a high coolant channel flowrate for a microchannel with W-ribs on the walls. CFD: computational fluid dynamics; Re: Reynolds number.

To understand this, analysis of CT scan results for the W-rib microchannel was conducted. Figure 11 compares a cross-section from the CT scan result to the design intent at that same location. For the CT scan analysis, a region identified as the rib protrusion from the surface (red) was isolated from the surrounding metal walls of the microchannel (green). When comparing to design intent, the sides of the as-manufactured rib are significantly rounded which likely reduces the sharp flow separations that normally occur around ribs. These separations are critical to the heat transfer performance of ribs, and it is quite likely that the as-manufactured geometry has reduced internal convective heat transfer, leading to warmer external metal temperature relative to the CFD.

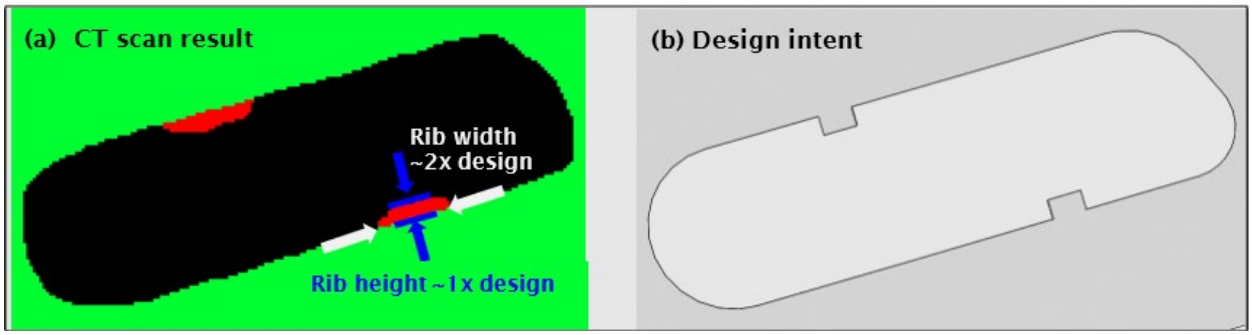

Figure 11. Comparison of computed tomography (CT) scan of an as-manufactured ribbed microchannel (a) to the design-intent shape (b) at a section in the middle of a microchannel.

Finally, conjugate CFD simulations were conducted of the microchannel with cylindrical pins that span between the inside and outside-facing walls of the microchannel. The resulting prediction of overall cooling effectiveness is shown in Figure 12, where the W-rib prediction is compared to the cylindrical pin prediction. In general, the overall cooling effectiveness is not significantly improved with cylindrical pins, despite their higher blockage of the microchannel. In fact, the pressure drop across the cylindrical pin microchannel is more than 12 times higher than for an empty microchannel, and more than 3 times higher than the pressure drop of the microchannel with W-ribs. This suggests that this type of design is not desirable since the pressure drop penalty is not offset by a significant improvement in cooling.

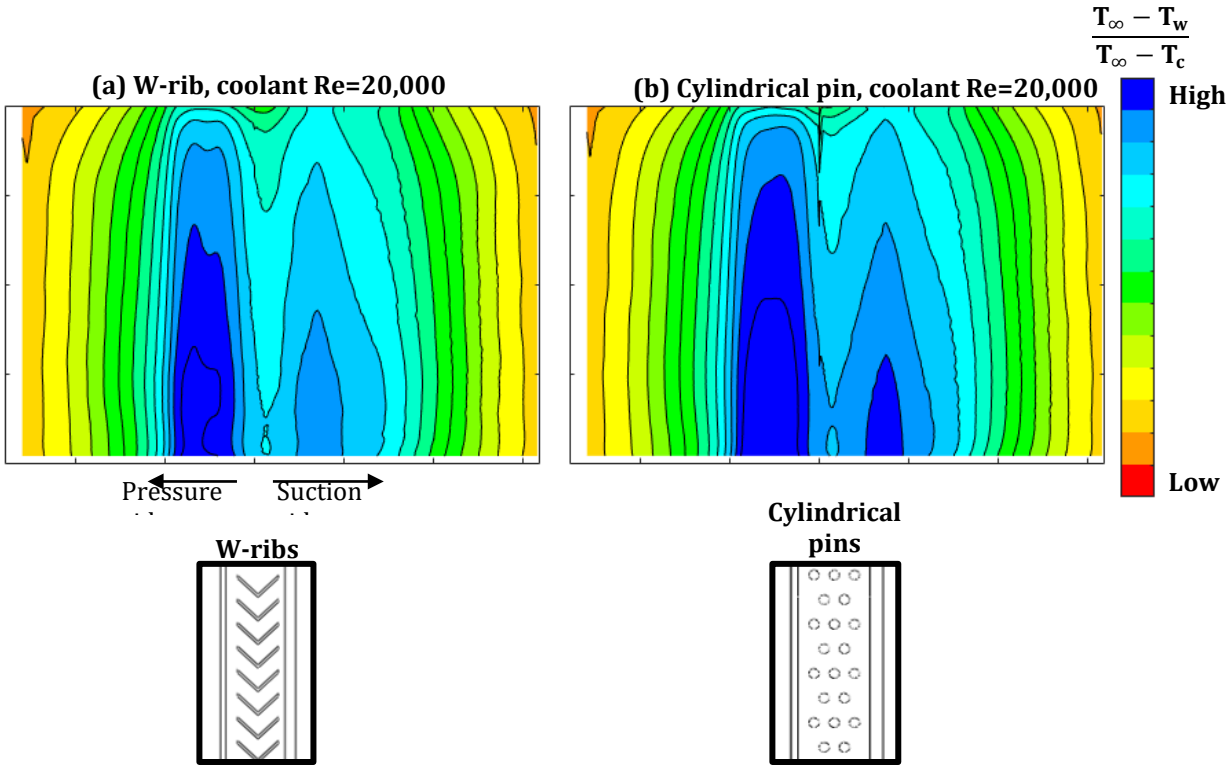

Figure 12. Comparison of overall cooling effectiveness prediction of W-rib design (a) to a cylindrical pin design (b) inside the microchannels.

Future work is investigating a modification to the W-rib cross section shape per observations of the as-manufactured design shown in Figure 11. This is being adjusted in the conjugate CFD so that new simulations can be run, to determine if the rib shape has a major impact on the overall cooling effectiveness.

Task 4 – Manufacture and Test AM NExT Blades with Varying Roughness

The Pennsylvania State University

Objective

The objective of this task is to quantify the impact of surface roughness for additively manufactured turbine blades. The START team will manufacture and evaluate a subset of turbine blades with methodical and controlled surface roughness levels. The specific roughness will be determined based on prior knowledge and informed by observations from fielded turbine engine hardware. Then, the roughness details will be applied to the National Experimental Turbine (NExT) blade geometry. Whereas prior work set out to understand differences strictly due to the roughness of the airfoil surfaces, this task will also evaluate the influence of roughness on the development of film cooling on the external surface of the airfoil. A combined approach evaluating external roughness levels with and without external film cooling will better differentiate

the connectivity between these effects. The subset of turbine blades will be assembled as a rainbow wheel, and the performance of the different roughness and cooling designs will be evaluated quantitatively using non-contact IR thermal imaging in the one-stage START facility.

Research Approach

A turbine "rainbow" test wheel has been designed to allow measurements of both cast Blades and AM Blades during the same experiment. This will ensure the test conditions are identical for the two different blade manufacturing processes, which will support understanding of the differences in manufacturing process on the heat transfer. The test wheel will also include different surface roughness levels on the printed blades, to help identify the impacts of internal cooling differences relative to external cooling differences. Figure 13 below shows a notional illustrative layout of the planned test wheel identifying blade configuration and surface roughness identified by color coordination.

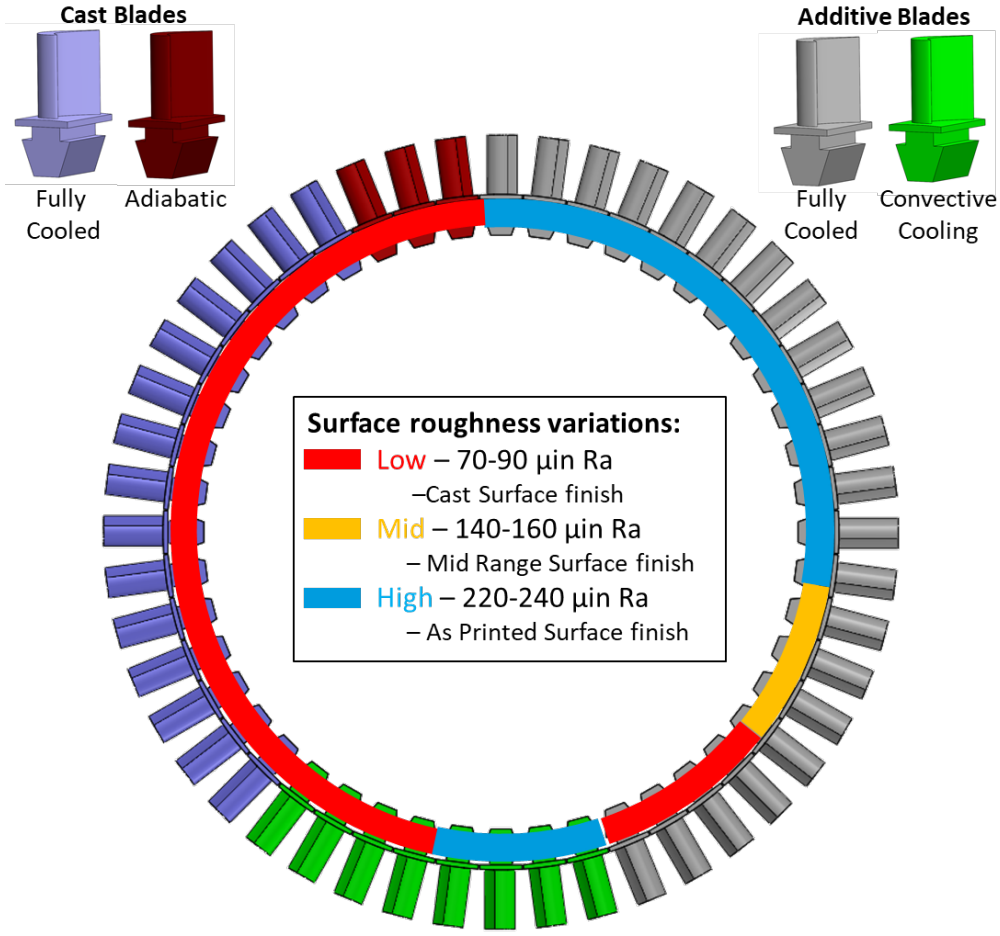

Figure 13. Example illustration of rainbow wheel configuration.

To facilitate modifying the printed blades to roughness levels equivalent to the cast blades, the cast blade surface roughness was measured using a surface roughness gage. The cast blade surface roughness average was determined to be an average of 80 µin Ra for these blades. The surface roughness of the as-printed blades was also measured using the surface roughness gage and determined to average 230 µin Ra—this value aligns with expectations and other measurements of as-printed AM components evaluated in prior programs. A subset of printed blades will have their surface roughness adjusted to align with the turbine test wheel configuration roughness plan, as demonstrated in

Figure 14. Following surface roughness modifications, the blades will transition to a vendor to have final hole configurations drilled as defined by the turbine test wheel configuration.

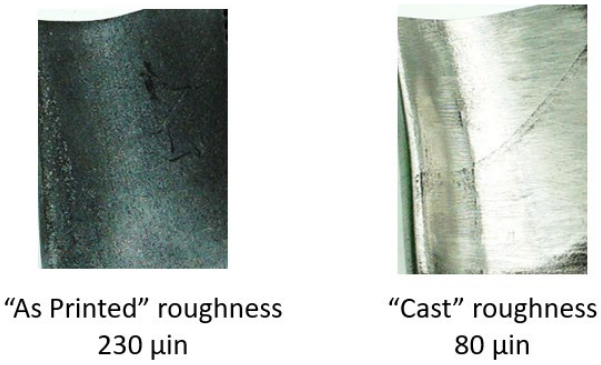

Figure 14. Additive manufacturing (AM) blade surface roughness comparison.

The configuration of the blades outlined in Figure 13 (cooled, convective, adiabatic) allows for more detailed understanding of the different aspects of the heat transfer occurring in the blades. The convective cooling configuration requires design work to ensure the convective blades have the appropriate internal flow characteristic. This design work is in progress and will enable final machining to be completed. The evaluation of external roughness on the behavior of film holes for AM turbine blades will be evaluated through testing in the START rig with a test schedule targeting a Q2 FY26 test window.

The rainbow wheel configuration that has been planned for this testing includes a convectively cooled blade configuration. The convectively cooled blade allows cooling flow to pass through the internal cooling channels of the blade and exit the blade without directly cooling the blade surface. This allows the internal cooling effectiveness to be studied. The design of the cooling flow exit features on the convective blades has been completed. The passage bleed holes sizes are established by matching the internal Reynolds numbers of each cooling passage with that of the film cooled blades thereby ensuring similar internal convective cooling characteristics between the two blade types. Figure 15 shows a cartoon of the cooling passages and their associated new bleed hole locations.

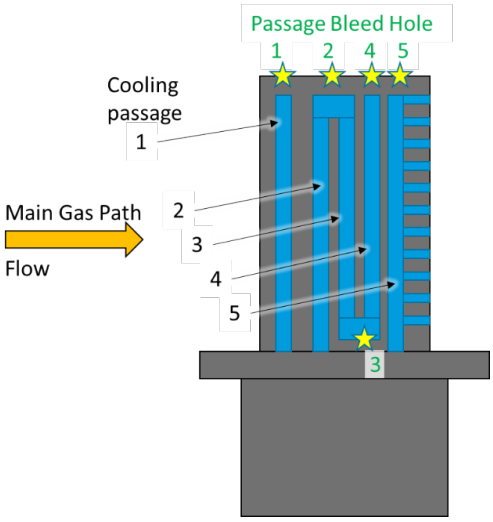

Figure 15. Convective Blade Cooling Bleed Holes.

For the external temperature of the blades to be determined using IR imaging, the surface of the blade has to be covered with a high emissivity coating. To understand the impact of the addition of this coating on surface roughness, a surface roughness comparator was coated using the same coating and technique that is used to coat the blades. Surface roughness measurements were taken before and after the coating was applied using a Taylor Hobson® Surtronic S-128 surface roughness tester. Figure 16 shows an image of the comparator plate taken post-paint. The green highlight boxes indicate the samples that were measured pre and post paint.

Coating the samples showed an impact on the surface roughness measurements from the applied coating. Table 1 shows that surface roughness less than ~100 Ra were made rougher, while surface roughness greater than ~100 were made less rough. The results of this test are driving additional studies to improve the coating process to reduce the impact on the surface roughness of the samples.

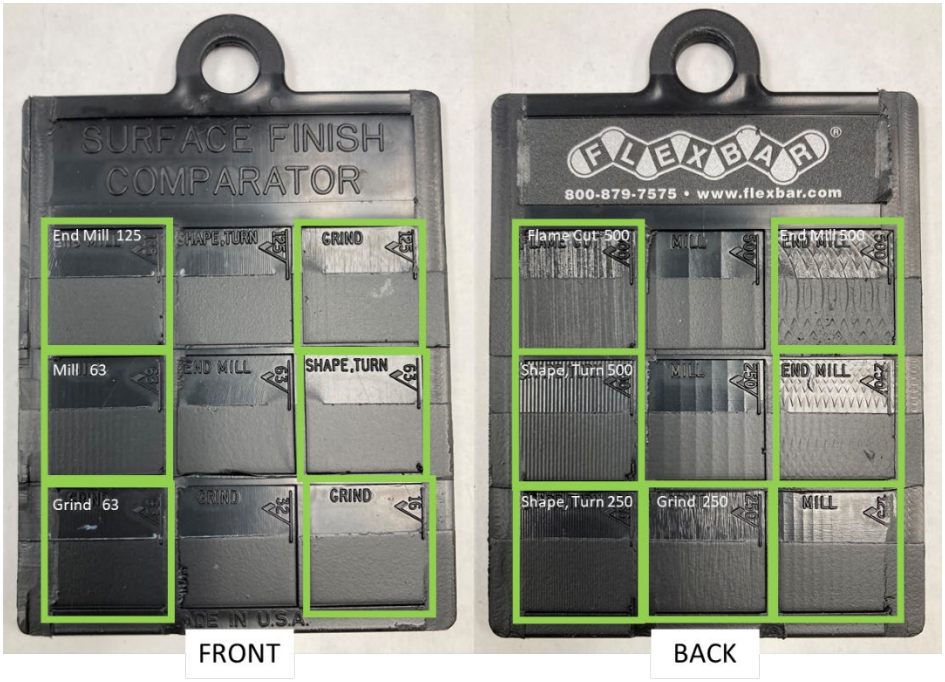

Figure 16. Comparator, Post-Paint.

®Taylor Hobson and Surtronic are registered trademarks of Taylor Hobson Limited, United Kingdom.

Table 1. Surface Roughness Measurements Pre- and Post-Paint.

Comparator Description	Ra [µin]	Pre-Paint	Post-Paint
Calibration Standard	236	240	240
Grind	16	20	43
Grind	63	37	63
Shape, Turn	63	40	37
Mill	63	30	43
Grind	125	57	67
End Mill	125	87	70
Mill	125	40	63
Grind	250	163	87
Shape, Turn	250	173	100
End Mill	250	83	63
Shape, Turn	500	253	160
End Mill	500	153	183
Flame Cut	500	247	177

Task 5 – Develop Correlations for Realistic Turbine Roughness

The Pennsylvania State University

Objective

The objective of this task is to evaluate the various roughness feature types using fielded engine parts to classify the various types of roughness levels and features. Experimental heat transfer measurements will be made on coupons with varied roughness scales and features based upon operational blades. AM coupons will be made to replicate those roughness types. It is important to note that having a fully metal coupon provides the needed boundary conditions for these heat transfer measurements of the convective heat transfer coefficients. As such, the approach of printing the three-dimensional (3D) coupons from metal is required rather than using the airfoils themselves. The printing also allows for a methodical approach whereby only the desired roughness scales are replicated thereby allowing for accurate correlations to be developed.

Research Approach

Using a laser microscope, optical scans were collected from three field-operated blades with different levels of deterioration to investigate degraded surface texture. On the pressure and suction sides, three scans were collected along the chord length at the upper midspan region of the blades. In addition, several scans were captured of the highly deteriorated regions near the leading edges including macroscale spallation and step-like features.

Rough surfaces are commonly characterized using the arithmetic mean height (S_a) which only quantifies average roughness magnitude. However, prior studies have shown that surface morphology and spatial orientation also influence aerothermal performance. To more comprehensively represent the surface roughness, a broader set of metrology parameters describing height, spatial structure, and shape were analyzed. The pressure sides of the blades displayed higher roughness magnitudes with more protruding deposition compared to the suction sides which had lower roughness magnitudes with more eroded features. The suction side roughness tended to have more directional textures along the flow direction. Regions near the leading edges and trailing edges were typically rougher compared to the mid chord regions.

To conduct heat transfer and pressure loss tests on these rough surfaces, the blade surface textures need to be replicated on flat plate test coupons. Because manufacturing microscale features is difficult, the first step was to evaluate 3D printing

resolution limits. Blade surface textures were replicated at-scale on flat plate test coupons with stereolithography (SLA) 3D printing. Figure 17 shows a height map of a blade surface next to its replicated 3D printed surface. Optical scans were also captured of the 3D printed surfaces to evaluate how closely replicated surfaces matched the original blade surfaces. Findings show that the SLA printer did not successfully resolve surface textures with small height magnitudes due to a minimum 25-micron layer thickness. Calculated metrology parameters deviated up to 2.5 times from the original blade surfaces. On the other hand, larger surface features at the meso- and macroscales, such as spallation pits, were better resolved. Metrology parameters for these replicated larger features closely matched on the real blade surfaces.

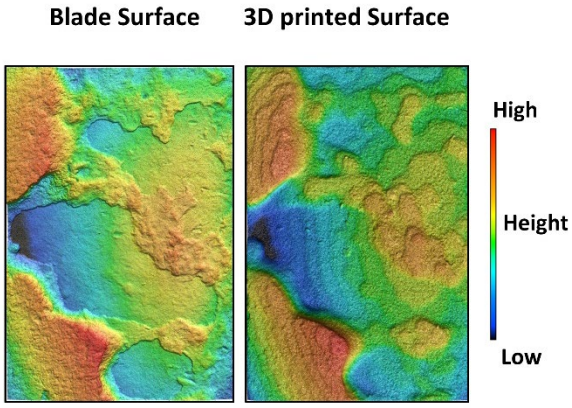

Figure 17. The high magnitude rough surface replicated using stereolithography three-dimensional (3D) printing.

Milestones

Milestone	Due date	Estimated date of completion	Actual date of completion	Status
Workplan	3/4/20	3/4/20	3/5/20	Completed
COE meeting 1	4/1/20	4/1/20		Cancelled
COE meeting 2	10/1/21	10/1/21	10/28–10/29/21	Completed
COE meeting 3	10/26/22	10/26/22	10/26–10/28/22	Completed
COE meeting 4	10/24/23	10/24/23	10/24/23	Completed
COE meeting 5	10/31/24	10/31/24	10/29-10/31/24	Completed
COE meeting 6	10/16/25	10/16/25	10/14-10/16/25	Completed
Annual report	12/31/25	12/31/25		
Project closeout	12/31/26	12/31/26		

Major Accomplishments

Following several years of planning and learning, significant learning continued this year under the project. In particular, data were collected from a second round of next-generation AM turbine blades for comparison with cast counterparts; AM NExT blades were manufactured and prepared for a rainbow wheel test program; and fundamental knowledge was gained in the impact of roughness for turbine heat transfer with applicability to fielded engine parts.

Publications

None.

Outreach Efforts

Research findings were presented throughout this review period as shown below.

Event	Date	Attendees
Bi-weekly calls	Every 2 weeks	Pratt & Whitney (PW) aerodynamics/durability engineers
Quarterly calls with turbine Original Equipment Manufacturers	Once per quarter	Industry partners: Solar, Siemens, Honeywell
National Aeronautics and Space Administration (NASA) university leadership initiative meeting	10/2/2024	NASA, FAA, PW, Collins, RTX Technology Research Center, Howard University, Georgia Institute of Technology
U.S. Department of Energy (DOE) National Experimental Turbine (NExT) annual review meeting	11/18/2024	DOE, NASA, PW, Solar, Siemens, Honeywell
Center of Excellence bi-annual meetings	1/30/2025 9/29/2025	Solar Turbine engineers
Research seminar visit	2/18/2025	Howmet Aerospace
Center of Excellence bi-annual meetings	12/9/2024 6/2/2025	PW aerodynamics/durability engineers and management

Awards

Dr. Reid Berdanier was elected as an Associate Fellow of the American Institute for Aeronautics and Astronautics (AIAA).
Dr. Karen Thole was awarded the 2025 Kate Gleason Award from the American Society of Mechanical Engineers (ASME).

Student Involvement

Nicholas Gailey was a PhD student who led the experimental analysis of AM turbine blades in the START rig. Nicholas completed his PhD in Summer 2025. Starting in September 2025, Nicholas is a turbine durability engineer at Pratt & Whitney.

Ethan Bonn, a PhD student, has been investigating AM turbine blade performance in the START rig since January 2025.

Benjamin Bizzak, a PhD student, has been participating in turbine blade preparation for Task 4 beginning Fall 2025.

Matthew Stuber, a MSME student, led the initial measurements of roughness for Task 5.

Abbigail Altland, a PhD Student, has led the detailed analysis of AM roughness effects for Task 5 beginning Fall 2025.

Plans for Next Period

- Conduct additional analysis of next-generation turbine blades manufactured through AM, supporting Task 1.
- Conduct further experimental and computational analysis of double-wall cooling designs in cascade performance, supporting Task 3.
- Build, test, and analysis of NExT turbine blades with AM roughness, supporting Task 4.
- Develop detailed roughness correlation models using available data, supporting Task 5.

Disclaimer

This research was funded by the FAA Office of Environment and Energy through ASCENT, the FAA Center of Excellence for Alternative Jet Fuels and the Environment, Project 056 through FAA Award Number 13-C-AJFE-PSU-126 under the supervision of Joshua Glottmann. Any opinions, findings, conclusions or recommendations expressed in this material are those of the authors and do not necessarily reflect the views of the FAA.